The Astrophysical Journal Letters, 897:L1 (7pp), 2020 July 1 https://doi.org/10.3847/2041-8213/ab9b7b

The State of the Heliosphere Revealed by Limb-halo Coronal Mass Ejections in Solar Cycles 23 and 24

Nat Gopalswamy[1], Sachiko Akiyama[1,2], and Seiji Yashiro[1,2]
[1] NASA Goddard Space Flight Center, Greenbelt, MD 20771, USA
[2] The Catholic University of America, Washington, DC 20624, USA
Received 2020 April 7; revised 2020 May 27; accepted 2020 June 10; published 2020 June 25

Abstract

We compare the properties of halo coronal mass ejections (CMEs) that originate close to the limb (within a central meridian distance range of 60°–~90°) during solar cycles 23 and 24 to quantify the effect of the heliospheric state on CME properties. There are 44 and 38 limb halos in cycles 23 and 24, respectively. Normalized to the cycle-averaged total sunspot number, there are 42% more limb halos in cycle 24. Although the limb halos as a population are very fast (average speed ~1464 km s^{-1}), cycle-24 halos are slower by ~26% than the cycle-23 halos. We introduce a new parameter, the heliocentric distance of the CME leading edge at the time a CME becomes a full halo; this height is significantly shorter in cycle 24 (by ~20%) and has a lower cutoff at ~6 R_s. These results show that cycle-24 CMEs become halos sooner and at a lower speed than the cycle-23 ones. On the other hand, the flare sizes are very similar in the two cycles, ruling out the possibility of eruption characteristics contributing to the differing CME properties. In summary, this study reveals the effect of the reduced total pressure in the heliosphere that allows cycle-24 CMEs to expand more and become halos sooner than in cycle 23. Our findings have important implications for the space-weather consequences of CMEs in cycle 25 (predicted to be similar to cycle 24) and for understanding the disparity in halo counts reported by automatic and manual catalogs.

Unified Astronomy Thesaurus concepts: Solar coronal mass ejections (310); Solar flares (1496); Solar energetic particles (1491); Radio bursts (1339); Heliosphere (711)

1. Introduction

Halo coronal mass ejections (CMEs) are normal CMEs that appear to surround the occulting disk of a coronagraph in sky-plane projection (Howard et al. 1982, 1985). The extended field of view (FOV) of the Solar and Heliospheric Observatory (SOHO) coronagraphs have shown that halo CMEs are an important subset of CMEs that are fast and wide on average (Webb et al. 2000; Webb 2002; Gopalswamy et al. 2003, 2007, 2010a; Zhao & Webb 2003; St. Cyr 2005; Lamy et al. 2019). The fraction of halo CMEs as an indicator of the energy of a CME population (Gopalswamy 2010), 60%–70% of CMEs associated with magnetic clouds (MCs), non-MCs, interplanetary Type II radio bursts, interplanetary shocks, intense geomagnetic storms, and large solar energetic particle (SEP), are halos. All CMEs (100%) associated with solar gamma-ray events lasting ⩾3 hr are halos (Gopalswamy et al. 2019a). Limb halos are asymmetric halos: eruptions from one limb of the Sun cause disturbances (shocks) above the opposite limb. The expansion of these CMEs must be enormous in that the associated shocks need to have an angular extent >180°. Limb halos are less geoeffective due to the glancing blow they deliver to Earth's magnetosphere (Gopalswamy et al. 2005, 2007), but occasionally they can produce intense geomagnetic storms due to their sheath (Huttunen et al. 2002; Gopalswamy et al. 2010b; Cid et al. 2012).

Comparing the widths of CMEs in cycles 23 and 24 associated with flares originating within 30° from the limb and having flare size ⩾C3.0, Gopalswamy et al. (2014a) reported that cycle-24 CMEs are wider, although the speeds are similar (average: 658 km s^{-1} in cycle 23 versus 688 km s^{-1} in cycle 24). Comparing all halo CMEs observed by SOHO coronagraphs in cycles 23 and 24 (irrespective of the source location) Gopalswamy et al. (2015b) reported that the halo numbers are similar in the two cycles unlike the sunspot number (SSN). The average halo–CME speeds are not different (933 km s^{-1} in cycle 23 versus 962 km s^{-1} in cycle 24), while the cycle-24 halos are widespread in longitude. These findings were attributed to back-reaction of the heliosphere on CME properties: CMEs expand anomalously in cycle 24 due to the reduced heliospheric pressure (Gopalswamy et al. 2014a). One of the implications of the inflated width is that cycle-24 CMEs should become halos at a lower speed and at shorter distances from the Sun. Disk halos are not useful for speed comparison because of the projection effects. Limb halos have minimal projection effects, so they are well suited. We now have large samples of limb halos in two whole cycles, so we can test this prediction (the limb-halo samples were small in Gopalswamy et al. 2014a). One might also wonder if the heliospheric state is solely responsible for the inflated CME widths in cycle 24. We answer this question by comparing the solar-source properties, using soft X-ray flare sizes, which are generally large for energetic CMEs such as halos. This work provides further evidence that the heliospheric state determines CME properties using a unique CME population—the limb halos.

2. Data

We use limb halos observed by SOHO's Large Angle and Spectrometric Coronagraph (LASCO; Brueckner et al. 1995) available at https://cdaw.gsfc.nasa.gov/CME_list/halo/halo.html (Gopalswamy et al. 2010a). The catalog lists CME sky-plane and space speeds, eruption location, flare start time, and

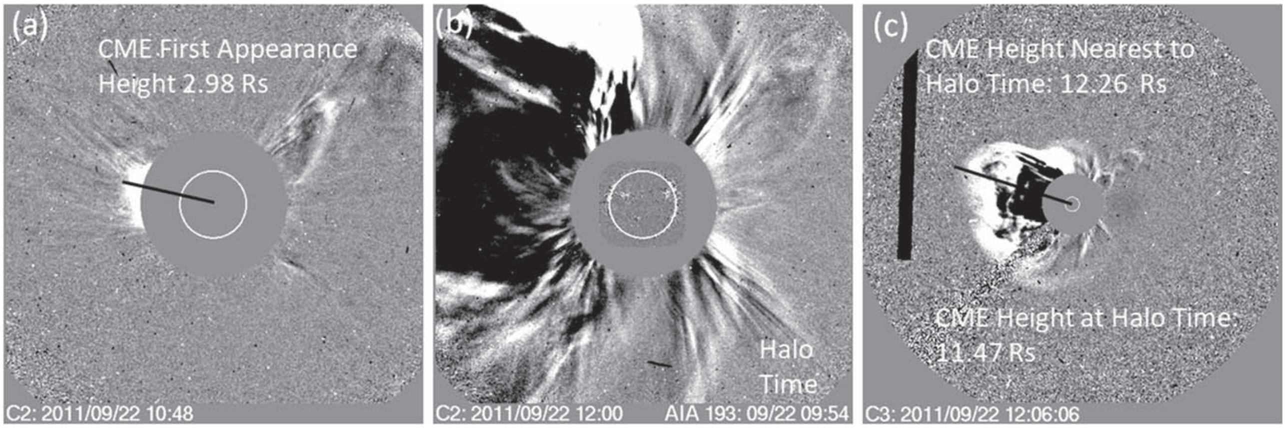

Figure 1. 2011 September 22 east-limb halo at (a) first appearance (10:48 UT) in LASCO/C2 FOV at a height of 2.98 R_s and (b) the "halo time" when the disturbances reach the west limb (11:36 UT). (c) 11:42 UT when the CME height is measured ($H = 12.26$ R_s) and extrapolated to the halo time using local speed (1905 km s^{-1}) to get the halo height (11.47 R_s).

soft X-ray flare size. We extract limb halos whose sources have a central meridian distance (CMD) in the range 60°–90°, although CMD = 90° include some behind the limb events. Backside events are readily identified using the Sun Earth Connection Coronal and Heliospheric Investigation (Howard et al. 2008) suit on board the Solar Terrestrial Relations Observatory (STEREO) only in cycle 24, so we stay with the single view. For the same reason, we do not consider halos observed by STEREO coronagraphs (Vourlidas et al. 2017).

Figure 1 shows an example: the 2011 September 22 halo, first appearing in the LASCO/C2 FOV at 10:48 UT, erupting from N09E89 in association with an X1.4 flare. The nose is the fastest moving section of the CME above the source region and always is readily identified in LASCO images as indicated in Figure 1. The CME sky-plane and space speeds are the same (1905 km s^{-1}) as the source is at the limb. The peak speed is ~2400 km s^{-1} determined from a Graduated Cylindrical Shell (Thernisien 2011) model fit to SOHO and STEREO images, but the average speed within the coronagraph FOV is close to the sky-plane speed (Gopalswamy et al. 2014b). At 11:36 UT, the CME-associated disturbances appeared on the west limb; this is the halo time (HT), when the CME leading edge (LE) has moved beyond LASCO/C2 FOV. In the 11:42 UT LASCO/C3 image, the LE is at ~12.26 R_s, which extrapolates to 11.47 R_s as the height at HT (h_{HT}). It is straightforward to determine h_{HT} because the nose is well within the LASCO/C3 FOV at HT. We followed this procedure to determine h_{HT} for 44 cycle-23 and 38 cycle-24 limb halos (see Table 1).

Table 1 lists the serial number, CME date, and first-appearance time in columns 1–3. Columns 4 and 5 give the eruption location and GOES soft X-ray flare size. h_{HT} is given in column 6. On 2010 August 10, the nominal cadence of LASCO C2 increased from 3 to 5 images hr^{-1}. One might think h_{HT} became smaller after the cadence change because our cycle-24 events occurred after this date. We computed h_{HT} by reducing the cycle-24 cadence to match that in cycle 23, given in parentheses (column 6). The sky-plane (V_{Sky}) and space speeds (V_{Sp}) are given in columns 7 and 8, respectively. Space speeds are expected be not more than 15% higher corresponding to an event originating at ~60° longitude. The data are incomplete (DG) for three cycle-23 halos. On 2003 November 11, a data gap from 13:54 to 15:30 UT prevented the determination of HT and h_{HT}. The 2005 January 20 CME was observed only in one LASCO/C2 frame; the subsequent images were corrupted by the intense energetic particle event (e.g., Gopalswamy et al. 2012). Although the halo nature can be discerned from the images, it is difficult to make meaningful measurements. When the 2006 December 6 CME appeared, the leading edge was beyond the LASCO/C2 FOV; there were no LASCO/C3 data, so no measurements are possible. We exclude these three events. Column 9 indicates whether a large SEP event is associated with the limb halos (Y—yes, N—no, M—minor, and HiB—high background due to previous events). Column 10 gives information on the associated type II radio burst from Wind/WAVES (Bougeret et al. 1995) observations (Gopalswamy et al. 2019b).[3] If a type II burst is present at decameter-hectometric (DH) wavelengths, the frequency range is noted. "N" indicates the absence of a type II burst. "Nm" indicates that a metric type II burst is associated with the CME, but not a DH type II burst.

3. Analysis and Results

In this section we compare the speed and h_{HT} distributions in solar cycles 23 and 24. We compare the cycle-23 h_{HT} with cycle-24 ones obtained using regular and reduced cadences. We perform Kolmogorov–Smirnov (KS) two-sample tests to compare CME and flare properties between the two cycles.

3.1. CME Speeds

Table 1 shows that the cycle-23 sky-plane (space) speeds range from 556 (563) km s^{-1} to 2657 (2662) km s^{-1}, with a similar range in cycle 24: 505 (516) km s^{-1} to 3163 (3163) km s^{-1}. Even the lowest speeds in the samples are higher than the average speed of the general population of CMEs (~450 km s^{-1}; see Gopalswamy 2010). For all limb halos in the two cycles the average sky-plane speed is 1464 ± 129 km s^{-1}, which is higher than that of all CMEs by a factor >3. The average sky-plane and space speeds are similar in each cycle, but they are quite different between the two cycles (Figure 2). The cycle-23 average sky-plane speed is 1637 ± 156 km s^{-1}, similar to the average space speed (1655 ± 156 km s^{-1}). Similarly, the cycle-24 average sky-plane speed is 1281 ± 202 km s^{-1}, not too different from the average space speed (1297 ± 202 km s^{-1}). The cycle-24 speed is thus ~28% smaller than that in cycle 23. The cycle-23 speed distribution is normal

[3] https://cdaw.gsfc.nasa.gov/CME_list/radio/waves_type2.html

Table 1
List of Limb-halo CMEs from Solar Cycles 23 and 24

#	CME Date (UT)	Time (UT)	Location	Flare Size	Halo Height (R_s)	V_{Sky} (km s^{-1})	V_{Sp} (km s^{-1})	SEP[a]	Type II[b] (MHz)
Cycle 23									
1	1997 Nov 6	12:10:41	S18W63	X9.4	8.97	1556	1604	Y	14–0.1
2	1998 Apr 23	05:55:22	S17E106	X1.4	9.62	1691	1691	HiB	14–0.2
3	1998 Nov 24	02:30:05	S28W103	X1.0	13.40	1798	1798	M	1–0.4
4	1999 Jul 25	13:31:21	N38W81	M2.4	17.67	1389	1392	N	0.2?
5	2000 Apr 4	16:32:37	N17W60	C9.7	13.57	1188	1372	Y	14–0.2
6	2000 May 5	15:50:05	S17W100	M1.5	10.77	1594	1594	M	14–2.5
7	2000 Oct 16	07:27:21	N03W108	M2.5	9.78	1336	1336	Y	14–1
8	2000 Oct 24	08:26:05	S23E70	C2.3	13.24	800	820	N	N
9	2000 Oct 25	08:26:05	N09W63	C4.0	7.98	770	813	Y	10–0.3
10	2001 Apr 1	11:26:06	S22E108	M5.5	13.72	1475	1475	HiB	DG
11	2001 Aug 19	06:06:05	N30W75	B8.4[c]	11.18	556	563	HiB	1–0.4
12	2001 Oct 1	05:30:05	S24W81	M9.1	10.19	1405	1409	Y	1–0.15
13	2001 Nov 22	20:30:33	S25W67	M3.8	13.55	1443	1472	Y	8–1
14	2001 Dec 14	09:06:06	N07E97	M3.5	14.22	1506	1507	N	0.7–0.3
15	2001 Dec 28	20:30:05	S24E104	X3.4	12.63	2216	2216	Y	14–0.35
16	2002 Jan 4	09:30:05	N38E87	C3.7	12.10	896	907	HiB	Nm
17	2002 Jan 14	05:35:07	S28W108	M4.4	11.05	1492	1492	Y	14–0.35
18	2002 Feb 20	06:30:05	N12W72	M5.1	10.80	952	965	Y	14–10?
19	2002 Mar 10	23:06:55	S22E113	M2.3	12.31	1429	1429	N	14–8
20	2002 Mar 22	11:06:05	S10W90	M1.6	15.79	1750	1750	Y	14–0.5
21	2002 Apr 21	01:27:20	S14W84	X1.5	20.25	2393	2396	Y	10–0.06
22	2002 Jul 19	16:30:05	S15E115	C2.9[d]	11.20	2047	2047	HiB	5–1
23	2002 Jul 20	22:06:09	S13E99	X3.3	13.74	1941	1941	M	10–2
24	2002 Jul 23	00:42:05	S13E72	X4.8	25.22[e]	2285	2318	HiB	11–0.4
25	2002 Aug 22	02:06:06	S07W62	M5.4	8.42	998	1034	Y	14–3.5
26	2002 Aug 24	01:27:19	S02W81	X3.1	12.09	1913	1920	Y	5–0.4
27	2002 Dec 8	23:54:05	S18E70	C2.5	13.76	1339	1361	N	DG
28	2003 May 31	02:30:19	S07W65	M9.3	19.65[e]	1835	1888	Y	3–0.15
29	2003 Jun 15	23:54:05	S07E80	X1.3	14.18	2053	2062	N	14–0.4
30	2003 Nov 4	19:54:05	S19W83	X28.	11.53	2657	2662	Y	10–0.2
31	2003 Nov 11	13:54:05	S03W61	M1.6	DG[f]	1315	1367	HiB	1–0.5?
32	2004 Jul 29	12:06:05	N00W90	C2.1	18.00	1180	1180	M	1–0.05
33	2005 Jan 20	06:54:05	N14W61	X7.1	DG[f]	…	…	Y	14–0.025
34	2005 Jun 3	12:32:10	N15E97	M1.0	14.48	1679	1679	N	10–0.27
35	2005 Jul 13	14:30:05	N11W90	M5.0	15.14	1423	1423	M	14–1
36	2005 Jul 14	10:54:05	N11W90	X1.2	17.31	2115	2115	Y	3–0.8
37	2005 Jul 27	04:54:05	N11E104	M3.7	14.08	1787	1787	Y	1–0.45
38	2005 Jul 30	06:50:28	N12E60	X1.3	9.73	1968	2043	Y	9–0.08
39	2005 Aug 22	17:30:05	S13W65	M5.6	10.77	2378	2445	Y	12–0.04
40	2005 Aug 23	14:54:05	S12W70	M2.7	18.45	1929	1929	HiB	13–0.2
41	2005 Sep 5	09:48:05	S07E119	C2.7[d]	12.50	2326	2334	N	1.5–0.06
42	2005 Sep 9	19:48:05	S12E67	X6.2	8.37	2257	2311	HiB	14–0.05
43	2006 Dec 6	20:12:05	S05E64	X6.5	DG[f]	…	…	Y	14–0.03
44	2007 Jan 25	06:54:04	S08E102	C6.3	14.97	1367	1367	N	14–0.09
Cycle 24									
1	2011 Aug 9	08:12:06	N17W69	X6.9	12.34 (1398)	1610	1640	Y	14–0.2
2	2011 Sep 22	10:48:06	N09E89	X1.4	11.47 (1357)	1905	1905	Y	14–0.07
3	2011 Oct 22	10:24:05	N25W77	M1.3	10.48 (1149)	1005	1011	Y	1.5–0.1
4	2012 Jan 16	03:12:10	N34E86	C6.5	9.08 (908)	1060	1060	N	3–0.9
5	2012 Jan 26	04:36:05	N41W84	C6.4	9.98(1084)	1194	1195	HiB	5–0.5?
6	2012 Jan 27	18:27:52	N27W78	X1.7	9.58 (958)	2508	2541	Y	14–0.15
7	2012 Feb 9	21:17:36	N18E80	B8.0[d]	11.21 (1121)	659	663	N	N[g]
8	2012 Feb 23	08:12:06	N27W71	B5.4	9.77 (1026)	505	516	N	N
9	2012 Mar 4	11:00:07	N19E61	M2.0	8.55 (855)	1306	1352	M	1–0.2
10	2012 Mar 13	17:36:05	N17W66	M7.9	13.16 (1316)	1884	1931	Y	14–0.2
11	2012 Apr 9	12:36:07	N20W65	C3.9	7.75 (874)	921	945	N	14–5
12	2012 May 17	01:48:05	N11W76	M5.1	12.63 (1263)	1582	1596	Y	14–0.3
13	2012 Jul 19	05:24:05	S13W88	M7.7	16.11 (1611)	1631	1631	Y	5–0.6
14	2012 Nov 8	02:36:06	N13E89	M1.7	11.81 (1181)	855	855	M	Nm

Table 1
(Continued)

#	CME Date (UT)	Time (UT)	Location	Flare Size	Halo Height (R_s)	$V_{\rm Sky}$ (km s^{-1})	$V_{\rm Sp}$ (km s^{-1})	SEP[a]	Type II[b] (MHz)
15	2012 Nov 27	02:36:05	N13E68	C6.0[d]	12.38 (1238)	844	874	N	N[g]
16	2013 May 13	02:00:05	N11E90	X1.7	11.28 (1255)	1270	1270	N	14-2
17	2013 May 13	16:07:55	N11E85	X2.8	16.75 (1675)	1850	1852	M	14-0.3
18	2013 May 14	01:25:51	N08E77	X3.2	19.12 (1912)	2625	2645	M	14–0.24
19	2013 May 15	01:48:05	N12E64	X1.2	10.78 (1078)	1366	1408	Y	14–0.3
20	2013 May 22	13:25:50	N15W70	M5.0	10.78 (1232)	1466	1491	Y	14–0.15
21	2013 Sep 24	20:36:05	N26E70	B6.5	10.92 (1092)	919	932	N	N[g]
22	2013 Oct 25	08:12:05	S08E73	X1.7	7.01 (701)	587	599	N	Nm
23	2013 Oct 25	15:12:09	S06E69	X2.1	10.79 (1079)	1081	1103	M	14–0.2
24	2013 Oct 28	02:24:05	N04W66	X1.0	9.67 (967)	695	726	M	Nm
25	2013 Oct 29	22:00:06	N05W89	X2.3	11.33 (1133)	1001	1001	M	Nm
26	2013 Nov 19	10:36:05	S14W70	X1.0	8.12 (812)	740	761	M	14–5
27	2014 Jan 20	22:00:05	S07E67	C3.6	8.58 (858)	721	750	N	14–8
28	2014 Feb 20	08:00:07	S15W73	M3.0	6.45 (750)	948	960	Y	12–7.7
29	2014 Feb 25	01:25:50	S12E82	X4.9	14.99 (1499)	2147	2153	Y	14–0.1
30	2014 Jun 10	13:30:23	S17E82	X1.5	11.99 (1348)	1469	1473	N	14–9
31	2014 Aug 24	12:36:05	S07E75	M5.9	6.65 (665)	551	569	N	Nm
32	2015 Feb 9	23:24:05	N12E61	M2.4	6.16 (763)	1106	1148	N	14–9?
33	2015 Mar 7	22:12:05	S19E74	M9.2	16.87 (1687)	1261	1304	N	14–8?
34	2015 Apr 23	09:36:05	N12W89	M1.1	9.39 (939)	857	864	M	3–1
35	2015 May 5	22:24:05	N15E79	X2.7	12.21 (1221)	715	721	N	2–0.5
36	2016 Jan 1	23:24:04	S25W82	M2.3	9.31 (1108)	1730	1734	Y	1.1–0.3
37	2017 Apr 18	19:48:05	N14E77	C5.5	14.54 (1543)	926	932	N	2–0.5?
38	2017 Sep 10	16:00:05	S09W90	X8.2[d]	13.87 (1413)	3163	3163	Y	14–0.15

Notes.
[a] Large SEP event (>10 MeV proton intensity ⩾10 particle flux unit, pfu; 1 pfu = 1 particle per cm^{-2} s^{-1} sr^{-1}): Y—yes, N—no, M—minor event (proton intensity <10 pfu), HiB—high background due to previous events.
[b] Type II burst: the frequency range in the DH domain, N—no DH Type II, m—metric type II.
[c] Flare size estimated from GOES light curve.
[d] The flare is partly occulted; the flare size is estimated from GOES data.
[e] Some uncertainty in the halo height due to lower cadence.
[f] Insufficient data to determine the height at halo time (DG—data gap).
[g] Associated with a quiescent filament eruption.

(median speed: 1594 km s^{-1}), while the cycle-24 distribution is lognormal (median speed: 1094 km s^{-1}). A KS comparison of the two sky-plane speeds yields a test statistic $D = 0.4365$ with a corresponding chance coincidence probability $p = 0.001$, indicating a highly significant D value. For sample sizes of 41 and 38 in the two cycles, the critical value $D_c = 0.3062$ at 95% confidence level, confirming that the speed difference between the cycles is significant ($D > D_c$). The D value is the same when space speeds are used in the test. Note that in the previous study that compared partial cycles, there was no speed difference between limb CMEs (cycle 23: 658 km s^{-1}; cycle 24: 688 km s^{-1}) associated with >C3.0 flares although the widths were significantly different (Gopalswamy et al. 2014a).

3.2. CME Leading-edge Height at Halo Time

Since the sky-plane and space speeds are similar, we determine $h_{\rm HT}$ using sky-plane measurements. The cycle-23 $h_{\rm HT}$ ranges from 7.98 R_s to 25.22 R_s (average: 13.33 ± 1.14 R_s); the cycle-24 $h_{\rm HT}$ ranges from 6.96 R_s to 19.12 R_s (average: 11.15 ± 0.99) R_s (Figure 3). The cycle-23 average $h_{\rm HT}$ is larger than that in cycle 24 by ∼19.6%. A KS test of the two $h_{\rm HT}$ distributions yields $D = 0.3280$ with a corresponding $p = 0.022$ indicating a statistically significant difference (at 95% confidence level, $D > D_c = 0.3062$). Reducing the cycle-24 image cadence to match that in cycle 23, the cycle-24 $h_{\rm HT}$ shows a small increase (∼4%): 11.60 ± 0.97 R_s (Figure 3(c)). Slower CMEs and smaller $h_{\rm HT}$ in cycle 24 indicate that halos are formed sooner and at lower speeds in cycle 24, confirming our prediction. The weak state of the heliosphere in cycle 24 allowing the CMEs to expand more and become halos sooner.

Figure 4 shows a weak but significant correlation between the speed and $h_{\rm HT}$. The weakest correlation is in cycle 23 with a correlation coefficient $r = 0.27$, which is still significant (the Pearson critical correlation coefficient (r_c) for a sample size of 41 is 0.26 at the 95% confidence level). In cycle 24, the correlation is stronger ($r = 0.51$ versus $r_c = 0.25$). This correlation simply means that with a given image cadence, faster CMEs will be observed in fewer frames within the FOV and therefore likely to be observed at larger heights at HT, which would have been estimated to be earlier if the cadence were higher. There is some indication of this effect shown in Figure 3. More interesting is the result that the data points in the two cycles are well separated around 1300 km s^{-1}, which is close to the average speed of cycle-24 CMEs. The cycle-24 (blue) data points are clustered at the lower left of the plot, while the cycle-23 (red) data points are at the upper right. The clustering suggests that cycle-24 CMEs become halos sooner at lower speeds, while the cycle-23 CMEs take longer and must be faster to become halos. In other words, the cycle-23 CMEs

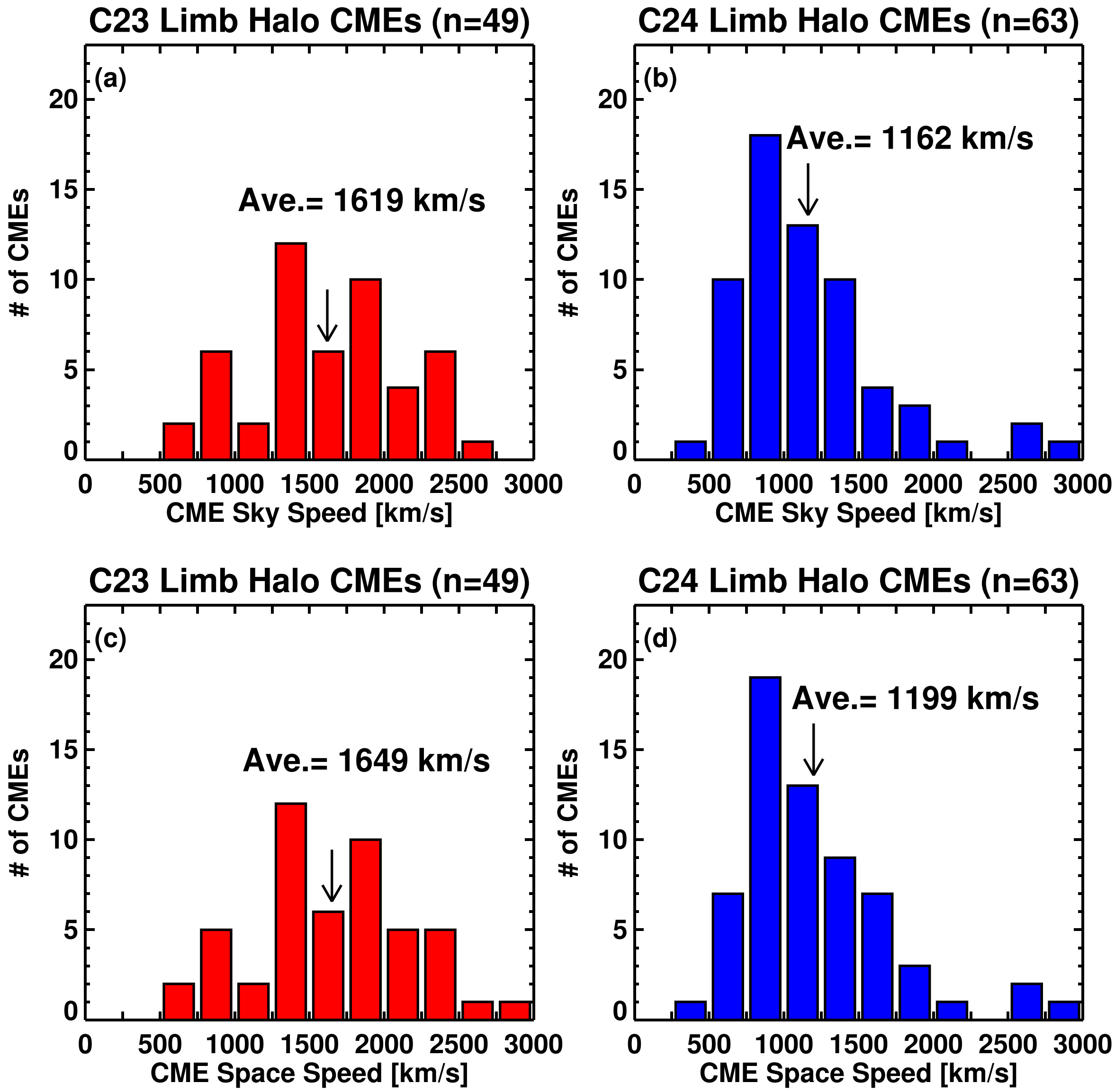

Figure 2. Sky-plane (a), (b) and space speed (c), (d) distributions of 41 cycle-23 and 38 cycle-24 halos. The distribution averages are noted.

need to work harder against the higher heliospheric total pressure to expand and become halos.

3.3. Flare Size Comparison

Flare sizes indicate how much of the released energy in an eruption is converted into thermal energy. The cycle-23 flare sizes range from B8.4 to X28 (15 X-, 19 M-, 9 C-, and 1 B-class flares) with a median of M4.7 (see Table 1). In cycle 24, the range is from B5.4 to X8.2 (16 X-, 13 M-, 6 C-, and 3 B-class flares) with a median of M6.8. The M- and X-class flares dominate in the two samples with similar fractions: 77% (SC 23) and 76% (SC 24). Evidently, the flare sizes are not significantly different between the two cycles. A KS test of the two sets of flare sizes yields $D = 0.1400$ with $p = 0.789$ indicating that the two flare-size distributions are not significantly different. At the 95% confidence level, $D < D_c = 0.3012$ for sample sizes of 44 (cycles 23) and 38 (cycle 24). Flares and CMEs are manifestations of the same energy release and products of the magnetic reconnection process in the source region. While the flare structure is confined to the Sun and not affected by the heliospheric state, CMEs propagate into the heliosphere and interact with it. Thus, similar flare sizes and differing CME properties are consistent with the differing heliospheric state in the two solar cycles.

3.4. Particle Acceleration

Large SEP events detected in space are indicative of particle acceleration by CME-driven shocks. While energetic electrons are also identified in space, a better indicator of them is the presence of type II radio bursts. Table 1 shows that 17 of the 25 (or 68%) cycle-23 western halos and 10 of the 17 (or 59%) in cycle 24 have SEP association. Only three eastern halos in each cycle have SEP association. In both cycles, there are many minor (M) and high-background (HiB) events. Only one western halo in cycle 23 and two in cycle 24 have no SEP association. The non-SEP CME in cycle 23 is from the 1999 July 25 high-latitude (N38W81) eruption. The two non-SEP CMEs in cycle 24 are slow: 505 km s^{-1} (2012 February 23) and 921 km s^{-1} (2012 April 9) compared to the typical speed

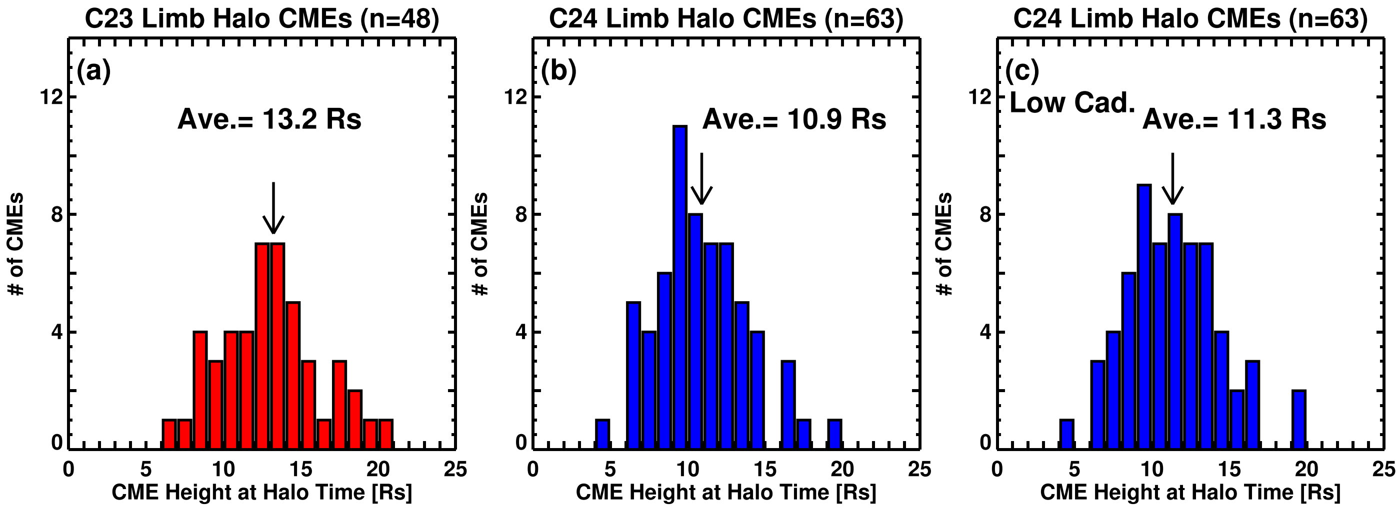

Figure 3. Distributions of halo heights (a) in cycle 23 and (b), (c) in cycle 24 with full and reduced cadences. The averages of the distributions are noted.

(∼1550 km s^{-1}) of CMEs associated with large SEP events (e.g., Gopalswamy 2018).

SEP events need to be magnetically connected to the observer in order to be detected; type II bursts do not have such a requirement. Only 2 of the 44 cycle-23 limb halos are not associated with DH type II bursts; they are slow (800 km s^{-1} on 2000 October 24; 896 km s^{-1} on 2002 January 4) compared to the average speed of CMEs associated with cycle-23 DH type II bursts (1219 km s^{-1}). The 2002 January 4 CME is associated with a metric type II burst, while the 2000 October 24 CME is radio-quiet. Nine cycle-24 halos have no DH type II association (see Table 1): five have metric type II bursts, three are quiescent filament-eruption events (which are only occasionally associated with DH type II bursts, Gopalswamy et al. 2015a), and the slowest cycle-24 halo (2012 February 23). The four radio-quiet halos are slow (505 to 919 km s^{-1}) compared CMEs associated with cycle-24 DH type II bursts (1059 km s^{-1}). Thus, an overwhelming majority of limb halos (cycle 23: 98%; cycle 24: 90%) have type II bursts indicative of electron acceleration.

4. Discussion and Summary

We analyzed large samples of limb-halo CMEs observed in cycles 23 and 24. We found that cycle-24 halos are slower than the cycle-23 ones. The limb CMEs that revealed wider width in cycle 24 did not show the speed difference (Gopalswamy et al. 2014a). We introduced a new parameter—the height at halo time is readily determined for limb halos, but not for disk halos (the CME nose is hidden by the occulting disk of the coronagraph). The cycle-24 halo heights are significantly smaller. Combined with the result that cycle-24 halos are slower, we conclude that halos form at shorter heliocentric distances at lower speeds. Furthermore, we ruled out the possibility that the difference in CME properties is due to solar-source characteristics represented by soft X-ray flare size. Thus, we can pin down the heliospheric state as the main cause of the anomalous CME expansion in cycle 24.

The number of limb halos (44) in cycle 23 is only slightly larger than the number (38) in cycle 24. This corresponds to a drop of only 14% in cycle 24. There was a 4 month SOHO data gap in cycle 23 (3 month in 1998 and one month in 1999). Assuming that the limb halos occurred at the cycle-averaged monthly rate (0.3 per month), we expect only one additional CME during the data gap. Then the drop is only 16%. This is much smaller than the 40% drop in the cycle-averaged total SSN from 81 to 49. Normalizing to SSN, we see that there are ∼42% more limb halos per SSN in cycle 24. This result was previously obtained by considering all LASCO halos in the first half of the two cycles (Gopalswamy et al. 2015b).

The effect of the heliospheric state on CMEs has important implications for space weather: lower geoeffectiveness is expected in SC 24 because lower speed and weaker CME magnetic field (due to expansion) result in a weaker storm. Furthermore, milder space weather is expected in cycle 25, which has been predicted to be similar to cycle 24. This study helps understand the disparity between manual and automatic catalogs in identifying halos. For example, the ARTEMIS catalog reported only 11 halos in cycle 23 (Lamy et al. 2019), while the SOHO/LASCO manual catalog reported nearly 400 halos. The lower cutoff of ∼6 R_s in the halo-height distribution (Figure 3) is very close to the outer edge of LASCO/C2 FOV. This might explain why automatic catalogs that use LASCO/C2 data, report very few halos. Our limb-halo data set will serve as a reference and ground truth to evaluate the success/failure of automatic catalogs.

The main results of this Letter can be summarized as follows:

1. Limb halos are one of the fastest of CME populations with an average speed of 1464 ± 129 km s^{-1}, with a high degree of SEP-event and type II-burst association and are mostly associated with M- and X-class flares.
2. The cycle-23 limb halos are significantly faster (1637 ± 164 km s^{-1}) than the cycle-24 ones (1281 ± 202 km s^{-1}).
3. A new parameter—the halo height characterizes the influence of the heliospheric state on CMEs. The average cycle-23 halo height (13.33 ± 1.14 R_s) is significantly larger than the cycle-24 value (11.15 ± 0.99 R_s).
4. The speed and halo-height differences indicate that cycle-24 CMEs become halos sooner at lower speeds, consistent with the effect of weak heliospheric state. In the initial study that reported wider CMEs in cycle 24 (Gopalswamy et al. 2014a), the limb CMEs had similar speeds.

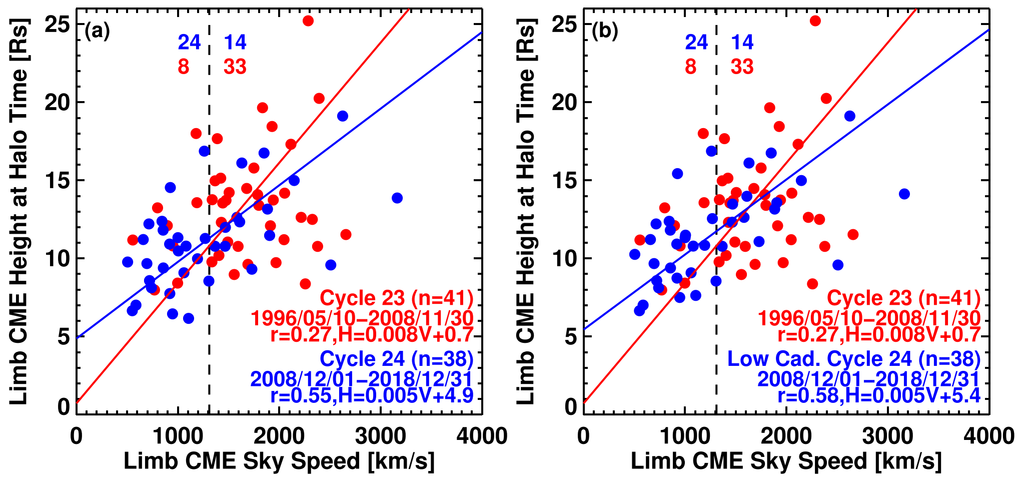

Figure 4. Scatter plots of h_{HT} vs. sky-plane speed in cycles 23 (red) and 24 (blue). (a) h_{HT} obtained using the actual cadences, and (b) cycle-24 h_{HT} obtained using reduced cadence. The best-fit lines and their equations are shown in red and blue for cycles 23 and 24, respectively (V: speed, H: halo height). The cycle-23 (red) and cycle-24 (blue) halos cluster on either side of ∼1300 km s^{-1}. The cycle-24 data points are generally at the lower left, while the cycle-23 data points are at the upper right, albeit some overlap.

5. The flare-size distributions in the two cycles are similar with median values of M4.7 (cycle 23) and M6.8 (cycles 24), indicating that the heliospheric state rather than the solar-source properties is responsible for the differing CME properties.
6. While there is a high degree of association between limb halos and shocks, the reduced association in cycle 24 is consistent with the reduced efficiency of particle acceleration.

This work benefited from NASA's open data policy in using SOHO, STEREO, and SDO data and NOAA's GOES X-ray data. SOHO is a joint project of ESA and NASA. STEREO is a mission in NASA's Solar Terrestrial Probes program. Work supported by NASA's LWS TR&T and heliophysics GI programs.

ORCID iDs

Nat Gopalswamy https://orcid.org/0000-0001-5894-9954
Sachiko Akiyama https://orcid.org/0000-0002-7281-1166
Seiji Yashiro https://orcid.org/0000-0002-6965-3785

References

Bougeret, J.-L., Kaiser, M. L., Kellogg, P. J., et al. 1995, SSRv, 71, 231
Brueckner, G. E., Howard, R. A., Koomen, M. J., et al. 1995, SoPh, 162, 357
Cid, C., Cremades, H., Aran, A., Mandrini, C., et al. 2012, JGRA, 117, A11102
Gopalswamy, N. 2010, in Proc. 20th National Solar Physics Meeting, 108
Gopalswamy, N. 2018, in Extreme Events in Geospace Origins, Predictability, and Consequences, ed. N. Buzulukova (New York: Elsevier), 37
Gopalswamy, N., Akiyama, S., Yashiro, S., et al. 2014a, GeoRL, 41, 2673
Gopalswamy, N., Lara, A., Yashiro, S., et al. 2003, in ESA SP-535, Solar Variability as an Input to the Earth's Environment, ed. A. Wilson (Noordwijk: ESA), 403
Gopalswamy, N., Mäkelä, P., Akiyama, S., et al. 2015a, ApJ, 808, 8
Gopalswamy, N., Mäkelä, P., Yashiro, S., et al. 2019a, JPhCS, 1332, 012004
Gopalswamy, N., Mäkelä, P., & Yashiro, S. 2019b, SunGe, 14, 91
Gopalswamy, N., Xie, H., Akiyama, S., et al. 2014b, EP&S, 66, 104
Gopalswamy, N., Xie, H., Akiyama, S., et al. 2015b, ApJL, 804, L23
Gopalswamy, N., Xie, H., Yashiro, S., et al. 2012, SSRv, 171, 23
Gopalswamy, N., Yashiro, S., & Akiyama, S. 2007, JGRA, 112, A06112
Gopalswamy, N., Yashiro, S., Liu, Y., et al. 2005, JGRA, 110, A09S15
Gopalswamy, N., Yashiro, S., Michalek, G., et al. 2010a, SunGe, 5, 7
Gopalswamy, N., Yashiro, S., Xie, H., et al. 2010b, in Solar Terrestrial (ST), Advances in Geosciences, Vol. 21, ed. W.-H. Ip & M. Duldig (Singapore: World Scientific), 71
Howard, R. A., Michels, D. J., Sheeley, N. R., et al. 1982, ApJL, 263, L101
Howard, R. A., Moses, J. D., Vourlidas, A., et al. 2008, SSRv, 136, 67
Howard, R. A., Sheeley, N. R., Jr., Michels, D. J., et al. 1985, JGR, 90, 8173
Huttunen, K. E. J., Koskinen, H. E. J., Pulkkinen, T. I., et al. 2002, JGRA, 107, 1440
Lamy, P. L., Floyd, O., Boclet, B., et al. 2019, SSRv, 215, 39
St. Cyr, O. C. 2005, EOSTr, 86, 281
Thernisien, A. 2011, ApJS, 194, 33
Vourlidas, A., Balmaceda, L. A., Stenborg, G., & Dal Lago, A. 2017, ApJ, 838, 141
Webb, D. F. 2002, in ESA SP-508, Proceedings of the SOHO 11 Symposium on From Solar Min to Max: Half a Solar Cycle with SOHO, ed. A. Wilson (Noordwijk: ESA), 409
Webb, D. F., Cliver, E. W., Crooker, N. U., et al. 2000, JGR, 105, 7491
Zhao, X. P., & Webb, D. F. 2003, JGRA, 108, 1234